Model-based Diagnosis of an Automotive Electric Power Generation and Storage System

Annalisa Scacchioli, *Member, IEEE*, Giorgio Rizzoni, *Fellow, IEEE*, Mutasim A. Salman, *Senior Member, IEEE*, Weiwu Li, Simona Onori, *Member, IEEE*, and Xiaodong Zhang, *Member, IEEE*

***Abstract*—This paper presents mathematical models, design and experimental validation, and calibration of a model-based diagnostic algorithm for an electric-power generation and storage automotive system, including a battery and an alternator with a rectifier and a voltage regulator. Mathematical models of these subsystems are derived, based on the physics of processes involved as characterized by time-varying nonlinear ordinary differential equations. The diagnostic problem focuses on detection and isolation of a specific set of alternator faults, including belt slipping, rectifier fault, and voltage regulator fault. The proposed diagnostic approach is based on the generation of residuals obtained using system models and comparing predicted and measured value of selected variables, including alternator output current, field voltage, and battery voltage. An equivalent input–output alternator model, which is used in the diagnostic scheme, is also formulated and parameterized. The test bench used for calibration of thresholds of the diagnostic algorithm and overall validation process are discussed. The effectiveness of the fault diagnosis algorithm and threshold selection is experimentally demonstrated.**

***Index Terms*—Automotive, electric power generator, electric power storage system, electrical systems, model-based diagnosis.**

NOMENCLATURE

Γ	Voltage controller.
$\Delta V_{\rm ref}$	Voltage regulator fault.
$\Delta\omega_e$	Belt slipping fault.
Φ	Phase angle between stator windings.
A	Battery's surface area.
$Ah_{\rm nominal}$	Battery nominal capacity.
C_0	Capacitance related to the dynamic phenomena of the battery.
E_0	Open-circuit voltage of the battery.
E_a, E_b, E_c	Inducted electromotive forces on windings a, b, c.
E_f	Inducted electromotive forces of the excitation field.
H_0, H_1	Hypothesis of no fault and faulty.
I_0	Current flow of the battery into resistance R_0.
I_B	Battery current.
I_L	Load current.
I_a, I_b, I_c	Current of phases a, b, c.
$I_{\rm dc}$	Alternator current.
$I_{\rm dc}^{\rm eq}$	Alternator current output from the equivalent alternator model.
$I_{\rm dc}^{\rm nom}$	Nominal value of alternator current output.
I_f	Alternator field current.
L_a, L_b, L_c	Self-inductances of the stator for phases a, b, c.
L_{ab}, L_{ba}	Stator–stator mutual inductances.
$L_{\rm ac}, L_{ca}$	Stator–stator mutual inductances.
L_{bc}, L_{cb}	Stator–stator mutual inductances.
L_{af}, L_{fa}	Stator–rotor mutual inductances.
L_{bf}, L_{fb}	Stator–rotor mutual inductances.
L_{cf}, L_{fc}	Stator–rotor mutual inductances.
L_f	Field winding self-inductance.
L_r	Self-inductance of the rotor.
L_s	Self-inductance of the stator.
L_{ss}	Stator–stator mutual inductance.
M	Peak stator–rotor mutual inductance.
P_D, P_I, P_M	Probability of detection, false alarm, and misdetection.
R	Internal ohmic resistance of the battery.
R_0	Overvoltage resistance of the battery model.
R_a, R_b, R_c	Resistances of stator windings.
R_f	Field winding resistance.
R_r	Rotor winding resistance.
R_s	Stator winding resistance.
SoC	Battery state of charge.
$\rm SoC_0$	Initial battery state of charge.
T	Battery temperature.
V_B	Battery voltage.
V_a, V_b, V_c	Voltage of the stator at terminals a, b, c.
V_{c0}	Voltage across the capacitor in the battery model.
$V_{\rm dc}$	Alternator voltage.
$V_{\rm dc}^{\rm eq}$	Alternator voltage output from the equivalent alternator model.
V_f	Alternator field voltage.
$V_f^{\rm eq}$	Field voltage output from the equivalent alternator model.
$V_{\rm ref}$	Alternator reference voltage.
$V_{\rm ref}^f$	Alternator reference voltage with voltage regulator fault.

Manuscript received May 27, 2011; revised August 27, 2012; accepted October 24, 2012. This paper was recommended by Associate Editor K. Hall.

A. Scacchioli is with the Faculty of the Department of Mechanical Engineering, School of Engineering, New York University, New York City, NY 11201 USA (e-mail: annalisa@poly.edu; annalisascacchioli@gmail.com).

G. Rizzoni and S. Onori are with the Center for Automotive Research, The Ohio State University, Columbus, OH 43210 USA (e-mail: rizzoni.1@osu.edu; onori.1@osu.edu).

M. A. Salman is with the General Motors Research and Development Center, Warren, MI 48088 USA (e-mail: mutasim.a.salman@gm.com).

W. Li was with the Center for Automotive Research, The Ohio State University, 930 Kinnear Road, Columbus, OH 43210 USA. He is now with Cummins Inc., Columbus, IN 47202 USA (e-mail: li.779@osu.edu).

X. Zhang is with the Faculty of the Department of Electrical Engineering, Wright State University, Dayton, OH 45435 USA (e-mail: xiaodong.zhang@wright.edu).

Digital Object Identifier 10.1109/TSMCC.2012.2235951

$V_{\mathrm{ref}}^{\mathrm{nom}}$	Nominal alternator reference voltage.
K_I, K_P	Gains of the voltage regulator.
λ	Vector of flux linkages.
$\mathbf{E}$	Vector of inducted electromotive forces on the stator's windings.
$\mathbf{I}$	Vector of phase currents.
$\mathbf{L}$	Matrix of inductances of the alternator.
$\mathbf{L_f}(\theta_\mathrm{e})$	Vector of mutual inductances stator field.
$\mathbf{R}$	Matrix of stator resistances.
$\mathbf{V}$	Vector of terminal voltages of windings of stator.
$\mathbf{f}$	Parameters' vector of the three-phase passive rectifier.
$\alpha, \beta, \gamma, \eta,$	Parameters of the equivalent alternator model.
κ, λ	Parameters of the equivalent alternator model.
$\lambda_a, \lambda_b, \lambda c$	Flux linkage of phases a, b, c.
ω_e	Electrical speed.
ω_e^f	Electrical frequency with belt slipping fault.
ω_m	Engine speed.
θ_e	Electrical angle.
θ_m	Engine phase angle.
c	Battery's lumped specific heat.
f_a, f_b, f_c	Parameters of the three-phase passive rectifier.
g_a, g_b, g_c	Conduction state of the diode in the branches a, b, c.
h_c	Convective heat transfer coefficient.
h	Selected threshold.
h_A	Heat transfer rate.
h_1	Optimal threshold related to belt slipping fault.
$h_2,$	Optimal threshold related to rectifier diode fault.
$h_{3,\mathrm{up}},$	Optimal threshold related to regulator fault.
$h_{3,\mathrm{down}}$	Optimal threshold related to regulator fault.
m	Battery mass.
m_c	Battery's convective heat losses.
p	Number of poles of the alternator.
pdf	Probability density function.
p_0, p_1	Probability density function for H_0 and H_1.
r	Random variable related to a residual.
r_1, r_2, r_3	Residuals.
sig_{r_1}	Fault signature of residual r_1.
sig_{r_2}	Fault signature of residual r_2.
sig_{r_3}	Fault signature of residual r_3.
k	Stator–rotor magnetic coupling.

I. Introduction

THIS introductory section provides motivation and background about the diagnostics of electrical automotive systems. The state-of-the-art of this research field and a description of objectives and main contributions of the paper are also provided at the end of the section.

A. Motivation

The past several decades have witnessed an exponential increase in the number and sophistication of electronic systems and subsystems in vehicles to meet various regulations and customer demands. Some of these subsystems are critical to measure vehicle performance and safety; on the other hand, others address comfort and convenience of the driving experience. Among automotive electrical systems, the electrical power generation and storage system, or EPGS system, is of critical importance.

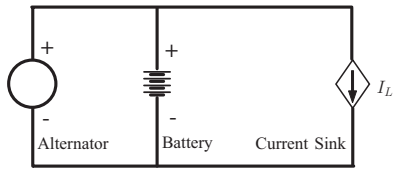

Fig. 1. Simplified EPGS automotive system diagram.

The EPGS system is designed to efficiently satisfy electrical power requirements of various subsystems, such as the engine electronic control unit (ECU), starter, headlights, radio, air conditioning, and steer-by-wire system. In this case, the EPGS system is actually the "engine" of all other electrical or electronic subsystems.

Fig. 1 shows a conceptual representation of the EPGS system in which the major subsystems—alternator and battery—are connected to a single-lumped load representing all other electrical/electronic subsystems. The alternator serves the purpose of satisfying all electrical load requirements in the steady state (when the engine is ON), while the battery satisfies transient and engine-off power requirements. In addition, the alternator also charges the battery as needed. As vehicles have become equipped with more complex and interdependent electronic systems, the number of electronic controls and software related to warranty problems has increased dramatically. In particular, due to the distributed nature of a vehicle electrical system, it is often very difficult to accurately identify the location of faults in general, and of intermittent faults in particular. This necessitates powerful diagnostics that automatically detect, isolate, and potentially compensate for faults. Such diagnostic capabilities can minimize down time, improve resource management via condition-based maintenance, and minimize warranty costs for the automotive manufacturer.

In published literature, one can find several studies on modeling of the electrical system, with particular attention given to the generator and battery [1]–[8]. Surprisingly, none of these focuses specifically on addressing the problem from a diagnostic perspective. There has been a lot of research on diagnosis or health monitoring of the energy storage system (or battery) [9]–[13], but very little work on diagnostics of the automotive power generation system (or alternator) has been reported in past years [14], [15]. Among results reported, even fewer are based on a systematic model-based approach [16], [17]. This paper focuses on the development of a model-based fault diagnostic method for the EPGS system. It provides a summary of a research project conducted by The Ohio State University Center for Automotive Research and the General Motors R&D; some of the results have been reported in [18]–[20]. Thus, this study presents a complete model-based fault diagnosis approach for the EPGS alternator subsystem, including its experimental validation. In this paper, we describe the EPGS system by time-varying nonlinear ordinary differential equations derived

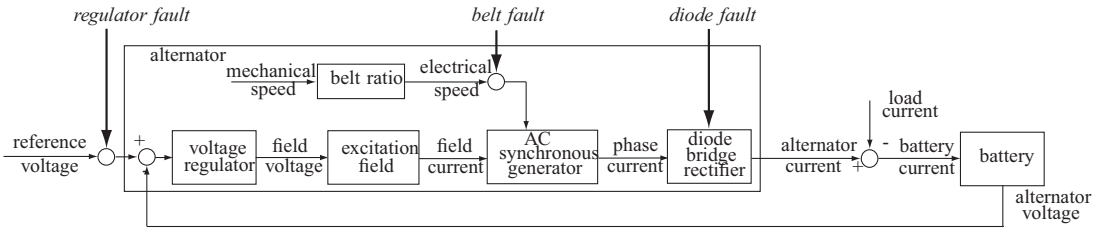

Fig. 2. Automotive EPGS system, including battery, alternator, and its subsystems with regulator, belt, and diode fault.

from the physics of processes involved. The alternator model is based on a model of an AC synchronous generator [1] derived using the principle of magnetic induction, a model of the diode bridge rectifier [4], and a proportional-integral (PI) control describing the voltage regulator. Battery dynamic equations utilize a second-order equivalent circuit to characterize electrical behavior and a first-order model to describe thermal behavior. The load is modeled by providing a prescribed load current profile, which is obtained from vehicle experimental data and known information about typical load currents associated with common accessories. In order to obtain a robust diagnostic algorithm, and in light of its implementation in the vehicle, our approach utilizes an equivalent mathematical linear time-invariant alternator model, where the equivalence of the two models is described in terms of input–output behavior.

B. Objectives and Contributions of This Paper

The diagnostic objectives of this study are summarized in the following with reference to Fig. 2.

1) *Belt fault*: an input fault that occurs when the alternator belt does not have proper tension to keep the alternator pulley rotating synchronously with the engine shaft; it may be caused by aging of the serpentine belt or incorrect installation, and its effect is a decrease in alternator output voltage, which in some cases can be compensated by the voltage regulator.
2) *Diode fault*: a failure of one of the bridge rectifier diodes, causing one branch of the circuit to be open; characteristics of this fault include a large ripple in output voltage and current, while its effect is a reduced output alternator current, caused by the lack of rectification in one of the phases.
3) *Regulator fault*: incorrect reference voltage caused, for example, by a software error in the ECU that leads to incorrect regulation.

In achieving these objectives, using a model-based diagnostic approach and adopting experimental validations, in this paper, we present the following contributions.

1) Development and experimental validation of an accurate model of the EPGS system, including analysis of uncertainty of the model.
2) Development and experimental validation of an equivalent linear model for the alternator and then for the complete EPGS system.
3) Design, implementation, and experimental validation of a robust diagnostics for belt and diode faults of EPGS.
4) Application of an optimal threshold selection and calibration method based on statistical analysis of appropriate experimental tests (design of experiment methodology).

This paper is organized as follows. Section II describes the complete EPGS mathematical system and its optimized simulation model with its experimental validation. Section III presents the EPGS diagnostic algorithm, including threshold selection and calibration. Section IV describes the experimental test bench used for the calibration and validation process of EPGS diagnostics, including a complete experimental validation example of EPGS diagnostics and a discussion of the results. Section V presents our concluding remarks and a short description of the future.

II. Electric Power Generation and Storage System Model

This section describes mathematical models of EPGS subsystems (alternator and battery) based on the physics of processes involved. They are extracted from existing literature. In particular, for the alternator, the AC synchronous generator is extracted from [1] and [3], and the three-phase diode bridge rectifier from [4], while the battery model is extracted from [21]. However, this paper presents two novel contributions in terms of system model: development and experimental validation of the accurate full EPGS model and development, identification, and experimental validation of an equivalent linear physical-based model of the alternator and, thus, of the EPGS system.

A. Electric Power Generation and Storage System Mathematical Model

1) Mathematical Model of the Alternator: The common automotive claw-pole alternator (see Fig. 3) is composed of the following subsystems: 1) three-phase AC synchronous generator; 2) three-phase diode bridge rectifier; and 3) voltage regulator (consisting of a switching control mechanism with a fixed reference voltage).

AC voltage generated by the alternator is rectified to provide the dc voltage required for supplying various electrical loads and for charging the battery. The *three-phase AC synchronous generator* model [1] is based on the following coupled circuit

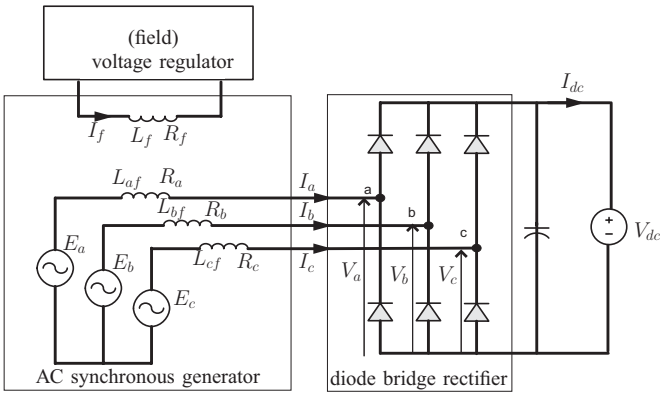

Fig. 3. Automotive alternator structure with its electrical subsystems: excitation field, three-phase AC synchronous generator, and diode bridge rectifier.

of the electrical dynamics of the stator and rotor:

$$E_a = R_a I_a + V_a \tag{1a}$$

$$E_b = R_b I_b + V_b \tag{1b}$$

$$E_c = R_c I_c + V_c \tag{1c}$$

$$E_f = R_f I_f + V_f \tag{1d}$$

where V_a, V_b, and V_c are the applied terminal voltages; V_f is the excitation field voltage; R_a, R_b, and R_c are the resistance of the stator winding; and R_f is the resistance of the field winding. E_a, E_b, and E_c are induced electromotive forces (EMF) of individual phases, and E_f is the inducted EMF of the excitation field, which are given by

$$E_a = \frac{d\lambda_a}{dt}, \quad E_b = \frac{d\lambda_b}{dt}, \quad E_c = \frac{d\lambda_c}{dt}, \quad E_f = -\frac{d\lambda_f}{dt} \tag{2}$$

where λ_a, λ_b, λ_c, and λ_f are flux linkages of individual phases, which are defined as

$$\lambda_a = -L_a I_a - L_{ab} I_b - L_{ac} I_c + L_{af}(\theta_e) I_f \tag{3a}$$

$$\lambda_b = -L_{ba} I_a - L_b I_b - L_{bc} I_c + L_{bf}(\theta_e) I_f \tag{3b}$$

$$\lambda_c = -L_{ca} I_a - L_{cb} I_b - L_c I_c + L_{cf}(\theta_e) I_f \tag{3c}$$

$$\lambda_f = L_f I_f - L_{fa}(\theta_e) I_a - L_{fb}(\theta_e) I_b - L_{fc}(\theta_e) I_c \tag{3d}$$

where L_a, L_b, and L_c are the self-inductance of the stator related to the three phases, and L_{ab}, L_{ba}, L_{ac}, L_{ca}, L_{bc}, and L_{cb} are the stator–stator mutual inductance, while the stator–rotor mutual inductances of the machine are described by

$$L_{af}(\theta_e) = L_{fa}(\theta_e) = M\cos(\theta_e) \tag{4a}$$

$$L_{bf}(\theta_e) = L_{fb}(\theta_e) = M\cos(\theta_e + \Phi) \tag{4b}$$

$$L_{cf}(\theta_e) = L_{fc}(\theta_e) = M\cos(\theta_e - \Phi) \tag{4c}$$

with M being the peak stator–rotor mutual inductance, Φ is the angle between stator windings, and θ_e is the phase angle of the alternator. The alternator's relation with the mechanical angular displacement θ_m (degrees) is described by

$$\theta_e = \frac{p}{2}\theta_m \tag{5}$$

where p is the number of poles of the alternator. Assuming a balanced machine, the balance equation for three-phase current is

$$I_a + I_b + I_c = 0. \tag{6}$$

The *three-phase diode bridge rectifier* model [4] associates switching function (g_a, g_b, g_c) with each of the bridge branches, representing the conduction state of the diode present in the branch. The switching function is equal to 1 if the diode is active or 0 if it is not. Its mathematical representation is described by

$$V_a = f_a V_{\rm dc}, \quad V_b = f_b V_{\rm dc}, \quad V_c = f_c V_{\rm dc} \tag{7}$$

$$f_a = \frac{2g_a - g_b - g_c}{3}, \quad f_b = \frac{2g_b - g_c - g_a}{3}$$

$$f_c = \frac{2g_c - g_a - g_b}{3} \tag{8}$$

$$I_{\rm dc} = g_a I_a + g_b I_b + g_c I_c. \tag{9}$$

The *voltage regulator* maintains alternator output voltage at a predetermined level across the engine's complete speed range, independent of load and engine speed. The specific set point for the regulator may vary as a function of operating conditions and is typically a lookup table. Without loss of generality, we consider the following PI controller voltage:

$$V_f = K_P(V_{\rm ref} - V_{\rm dc}) + K_I \int_{t_0}^{t} (V_{\rm ref} - V_{\rm dc})dt \tag{10}$$

where field voltage V_f is saturated at $V_{\rm dc}$, while K_P and K_I are appropriate gains.

Given the following matrix-vector notation:

$$\mathbf{I} = \begin{pmatrix} I_a \\ I_b \\ I_c \end{pmatrix}, \quad \mathbf{V} = \begin{pmatrix} V_a \\ V_b \\ V_c \end{pmatrix}, \quad \mathbf{E} = \begin{pmatrix} E_a \\ E_b \\ E_c \end{pmatrix}$$

$$\mathbf{f} = \begin{pmatrix} f_a \\ f_b \\ f_c \end{pmatrix}, \quad \lambda = \begin{pmatrix} \lambda_a \\ \lambda_b \\ \lambda_c \end{pmatrix}, \quad \mathbf{L_f}(\theta_e) = \begin{pmatrix} L_{af}(\theta_e) \\ L_{af}(\theta_e) \\ L_{af}(\theta_e) \end{pmatrix}$$

$$\mathbf{R} = \begin{pmatrix} R_s & 0 & 0 \\ 0 & R_s & 0 \\ 0 & 0 & R_s \end{pmatrix}, \quad \mathbf{L} = \begin{pmatrix} L_s & L_{ss} & L_{ss} \\ L_{ss} & L_s & L_{ss} \\ L_{ss} & L_{ss} & L_s \end{pmatrix}$$

and after assuming a balanced three-phase circuit

$$R_a = R_b = R_c = R_s \tag{11a}$$

$$L_a = L_b = L_c = L_s \tag{11b}$$

$$L_{ab} = L_{ba} = L_{ac} = L_{ca} = L_{bc} = L_{cb} = L_{ss} \tag{11c}$$

simpler and more compact mathematical expressions of the alternator and of the excitation field can be presented as follows:

$$\mathbf{E} = \mathbf{RI} + \mathbf{V} \tag{12a}$$

$$\mathbf{E} = \frac{d}{dt}\lambda \tag{12b}$$

$$\lambda = -\mathbf{LI} + \mathbf{L_f}^T(\theta_e) I_f \tag{12c}$$

$$\mathbf{V} = \mathbf{f} V_{\rm dc} \tag{12d}$$

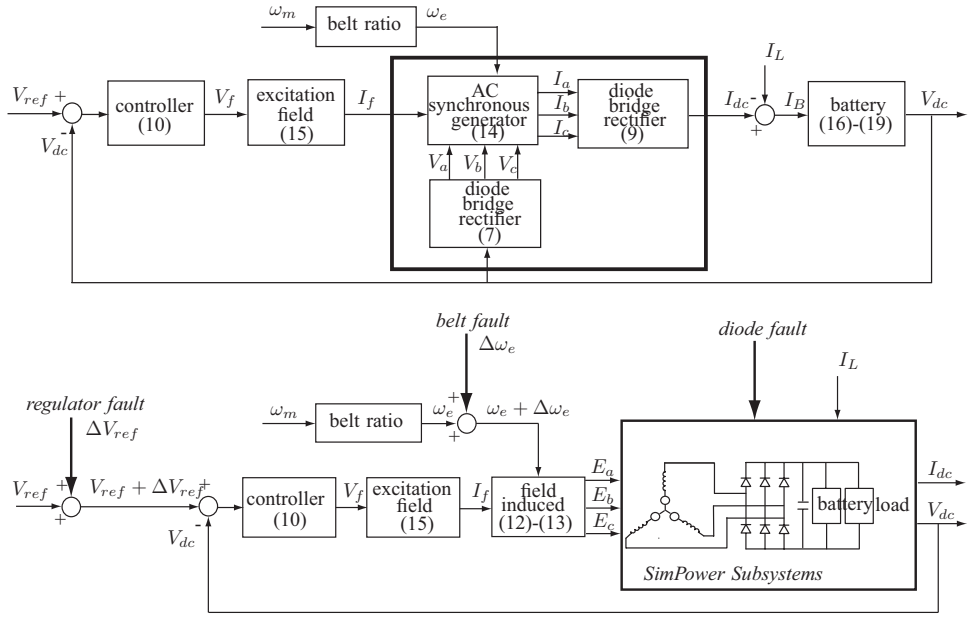

Fig. 4. EPGS model. (Top) Functional block diagram of the automotive EPGS mathematical model, including alternator and battery. (Bottom) Schematics of the automotive EPGS simulation model with fault injection.

and

$$E_f = R_f I_f + V_f \tag{13a}$$

$$E_f = -\frac{d}{dt}\lambda_f \tag{13b}$$

$$\lambda_f = -\mathbf{L_f}^T(\theta_e)\mathbf{I} + L_f I_f \tag{13c}$$

$$V_f = \Gamma(V_{\rm dc}) \tag{13d}$$

where Γ denotes PI controller voltage. Finally, rotor–stator dynamic is given by

$$\dot{\mathbf{I}} = -\mathbf{L}^{-1}(\mathbf{RI} + \mathbf{V}) + \mathbf{L}^{-1}\Big(\frac{d}{d\theta_e}\mathbf{L_f}(\theta_e)\omega_e I_f + \mathbf{L_f}(\theta_e)\dot{I}_f\Big) \tag{14}$$

after substituting values of (12a) and (12b) into the derivative of (12c). Similarly, from (13), one gets the following dynamic of the field circuit:

$$\dot{I}_f = -\frac{R_f}{L_f}I_f - \frac{1}{L_f}V_f + \frac{1}{L_f}(\mathbf{I} + \mathbf{L_f}^T(\theta_e)\dot{\mathbf{I}}). \tag{15}$$

Note that this model does not lend itself to the development of simple diagnostic algorithms, for example, based on observers, due to its nonlinear and hybrid nature.

2) Mathematical Model of the Battery: For the aim of this study, the battery system model is given by 1) an electric model, 2) SoC model, and 3) a thermal model. The *battery electric* model [21], which is based on an equivalent Thévenin circuit (see Fig. 5), is described by

$$V_B = E_0 - RI_B - V_{C_0} \tag{16a}$$

$$\dot{V}_{C_0} = -\frac{V_{C_0}}{R_0 C_0} \tag{16b}$$

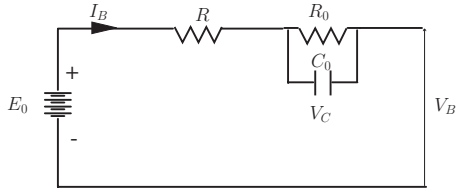

Fig. 5. Electrical battery model based on the equivalent Thévenin circuit.

where I_B is the battery current (positive during charging and negative during discharging), V_B is the battery voltage, R is the battery internal ohmic resistance, R_0 is the overvoltage resistance, C_0 is the capacitance, and E_0 is the open-circuit voltage.

The SoC is described by

$$\text{SoC} = \text{SoC}_0 - \frac{1}{Ah_{\rm nominal}}\int_{t_0}^{t} I_B\,dt \tag{17}$$

where I_B is the battery current during charging or discharging, t is the related time, $Ah_{\rm nominal}$ is the nominal battery capacity, and SoC_0 is the initial SoC at t_0.

The *battery thermal model* is described by a lumped first-order model

$$\dot{T} = -\frac{h_c A}{mc}(T - T_\infty) + \frac{R}{mc}I_B^2 + \frac{R_0}{mc}I_0^2 \tag{18}$$

where m is the mass of the battery, c is the battery's lumped specific heat, h_c is the convective heat transfer coefficient, A is the surface area, T is battery temperature, assumed uniform, and I_0 is the current flow into resistance R_0. Introducing, $T_1 = T - T_\infty$, (18) becomes

$$\dot{T}_1 = -\frac{h_c A}{mc}T_1 + \frac{R}{mc}I_B^2 + \frac{R_0}{mc}I_0^2. \tag{19}$$

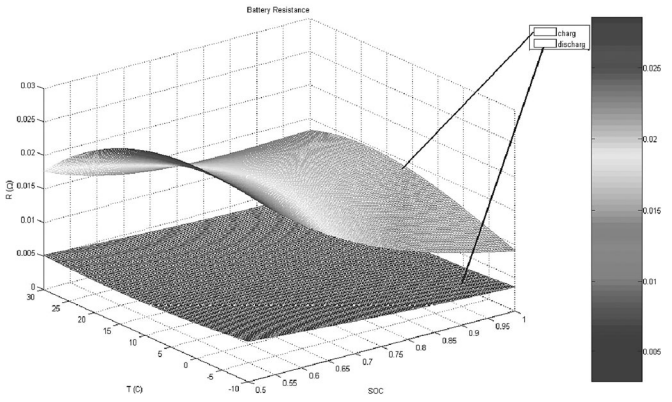

Fig. 6. Battery internal ohmic resistance R for charging and discharging (blue shape) phases.

The parameters, E_0, C_0, R, and R_0 of (16)–(19), are functions of battery state of charge SoC, battery temperature T, and battery current I_B. A typical shape of the battery internal ohmic resistance R during charging and discharging is shown in Fig. 6. Details are in [21]. While this study is not concerned with diagnostics battery faults, it is important for the accuracy and robustness of the EPGS diagnostics system to include a realistic battery model in the overall system model.

B. Electric Power Generation and Storage System Simulation Model With Faults

The highly nonlinear and complex EPGS mathematical model described through (2)–(19) and shown in the block diagram on the top of Fig. 4 has been implemented in Simulink. The Simulink model was partly validated using a Saber simulator, EPSSIM, made available by GM R&D [18]. A second EPGS simulation model (see the bottom of Fig. 4) with a modified alternator model was also developed by using the SimPowerSystems library of Simulink together with Simulink itself.

The SimPowerSystems is a module-based power system simulation tool available in MATLAB. It can be combined seamlessly with analytical equations to realize simulation of complex systems. A big advantage of utilizing SimPowerSystems in the EPGS simulation model is the possibility of simulating the diode bridge rectifier subsystem, which provides extreme flexibility and convenience for simulation of the diode fault.

In the final automotive EPGS system simulator (see the bottom of Fig. 4), the alternator stator, rectifier, battery, and load model are implemented and embedded in SimPowerSystems, while the controller, excitation field, and the induced electromagnetic field (EMF) are implemented in Simulink. The serpentine belt slip fault, rectifier diode open fault, and voltage regulator fault are considered as automotive EPGS system faults. These faults can easily be implemented by changing only one parameter or open-circuiting one diode.

The belt slipping fault and voltage regulator fault are described as additive faults through $\omega_e^f = \omega_e + \Delta\omega_e$ and $V_{\rm ref}^f = V_{\rm ref} + \Delta V_{\rm ref}$, respectively. The rectifier diode open fault is directly implemented in SimPower. Fault injection is also illustrated in the bottom of Fig. 4. Identified parameters of the alternator are given in Table I.

The EPGS system model was validated using experimental data gathered from the test bench, which is described in Section IV-A. Engine speed and load profiles (shown in Fig. 8) were designed to test the alternator's response to load changes and acceleration at low, medium, and high engine speeds. Experimental data are filtered (in MATLAB) using a fourth-order low-pass digital *Butterworth filter* with a cutoff frequency, of 2.5 Hz. With such a cutoff frequency, dominant dynamics of the system in response to load transients are preserved. Fig. 7 shows experimental and simulation results for alternator current, alternator voltage, and field voltage, suggesting that the implemented automotive EPGS simulator is an acceptable representation of described automotive EPGS system dynamics.

III. Electric Power Generation and Storage Diagnosis Problem and Proposed Approach

In this section, we present an equivalent but simplified EPGS model that is used for the development of a model-based diagnostic algorithm based on a parity equation approach. An optimal threshold selection and calibration approach are also proposed in this section.

Fault detection and isolation (FDI) aims to recognize faulty behavior of components based on measured signals. A typical approach of FDI is analytical redundancy: constructing residual generators based on models of the system (for example, through the design of state observers or parity equations). Unfortunately, the complexity of the EPGS system is significant. For the alternator system, the combination of nonlinear dynamics of the three-phase generator with the switched, state-dependent behavior of the diode bridge rectifier and with varying-time parameters of the battery makes the design of such residual generators very challenging. For example, linearization is impossible in the presence of hard nonlinearities. A direct nonlinear parity equation or observer design for such a complex nonlinear switch system is also extremely difficult. In [22], the authors present several nonlinear sliding model observer-based methods for alternator EMF estimation. However, those methods are dependent on the availability of alternator phase current, which is not available in our case.

A. Need of an Equivalent Alternator Model

In light of its implementation in a vehicle, the approach proposed in this study utilizes an equivalent mathematical linear time-invariant alternator model. The equivalence of the two models is in terms of input–output behavior. Equivalent representation is made possible by replacement of the AC synchronous generator and diode bridge rectifier with an equivalent DC generator. Input–output behavior of the subsystem in the big black box in Fig. 11 is functionally similar to that of a DC machine.

An equivalent excitation field (20a) and a first-order linearized model based on a DC generator equation (20b) describe the

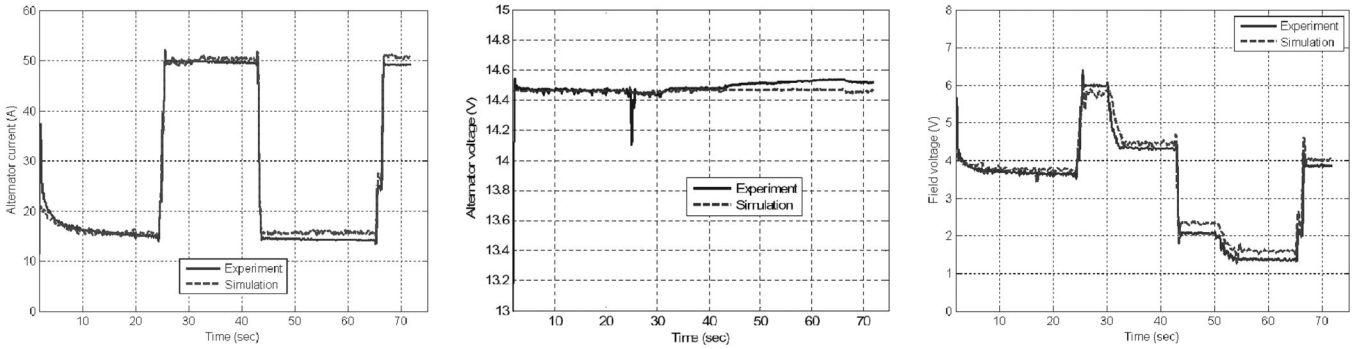

Fig. 7. Automotive EPGS full model validation: (left) field voltage, (middle) alternator current, and (right) alternator voltage.

input–output behavior of this subsystem

$$\dot{I}_f = -\alpha I_f + \beta V_f \tag{20a}$$

$$\dot{I}_{\rm dc} = -\gamma I_{\rm dc} + \eta \omega_e + \kappa I_f - \lambda V_{\rm dc}. \tag{20b}$$

In (20), input signals are engine speed ω_e, field voltage V_f, and alternator voltage $V_{\rm dc}$, while battery current I_B is the output—all these variables are available through specific sensors in the vehicle, while the six parameters α, β, γ, η, κ, and λ are determined using MATLAB/Simulink identification methods, through a parameters' estimation procedure based on four overlapping regions (see Fig. 9).

The input dataset is subdivided into four regions, each of them is uniquely associated with a parameter set, and a lookup table with these parameters is selected dynamically by using engine speed as the scheduling variable. The average engine speed in each region is mapped to the parameter value calculated in that region using a 700 r/min separation between data points. Linear interpolation and extrapolation are utilized to approximate parameter values between table entries or beyond table bounds. The parameter interpolation approach allowed the equivalent linear model to adequately reproduce behavior of the nonlinear model under a wide range of operating conditions. During the EPGS equivalent model validation procedure, we compared response of the EPGS system based on the nonlinear model of the alternator with response of the EPGS system based on the equivalent linear alternator model with an input dataset different from that used during optimization. Load current and engine speed profiles simulate power accessories turned ON and OFF during two common steady-state engine speeds at idle (850 r/min) and at cruising (2100 r/min), as depicted in Fig. 8.

Validation results of Fig. 10 show that the equivalent model works reasonably well in each range.

TABLE I
PARAMETERS OF THE ALTERNATOR

Parameter	*Description*	*Value*	*Unit*
R_s	stator winding resistance	30	mΩ
R_r	rotor winding resistance	3.44	Ω
L_s	self inductance of the stator	198	μH
L_r	self inductance of the rotor	500	mH
L_{ss}	stator-stator mutual inductance	90	μH
M	peak stator-rotor mutual inductance	230	μH
p	number of poles	12	
k	stator-rotor magnetic coupling	0.99	
Φ	phase angle between stator windings	120	^{0}

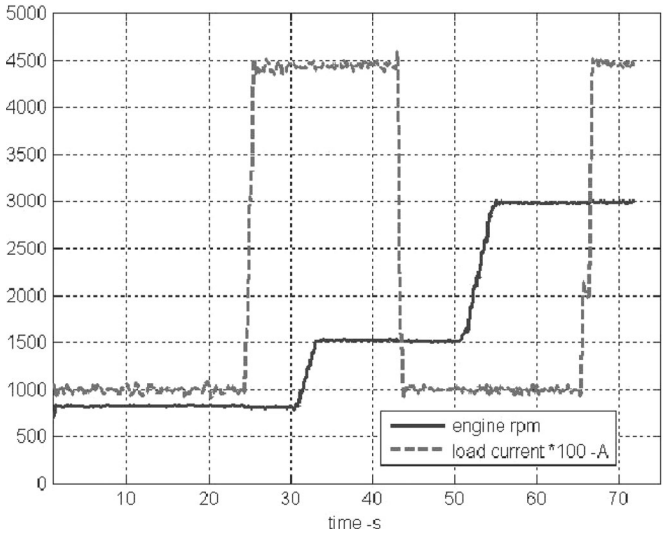

Fig. 8. Automotive EPGS full model and EPGS equivalent model validation: load current and engine speed input profiles used for validation of both the full and the equivalent EPGS model.

B. Fault Diagnosis Algorithm Design

The designed fault diagnosis algorithm proposed in this paper uses a parity equation approach based on an equivalent model and compares behavior of the alternator with the behavior of the equivalent model to produce residuals that contain information about faults. The residuals used for FDI are defined as

$$r_1 = (I_{\rm dc} - I_{\rm dc}^{\rm eq})/I_{\rm dc}^{\rm nom} \tag{21a}$$

$$r_2 = (V_f - V_f^{\rm eq})/V_{\rm ref}^{\rm nom} \tag{21b}$$

$$r_3 = (V_{\rm dc} - V_{\rm dc}^{\rm eq})/V_{\rm ref}^{\rm nom} \tag{21c}$$

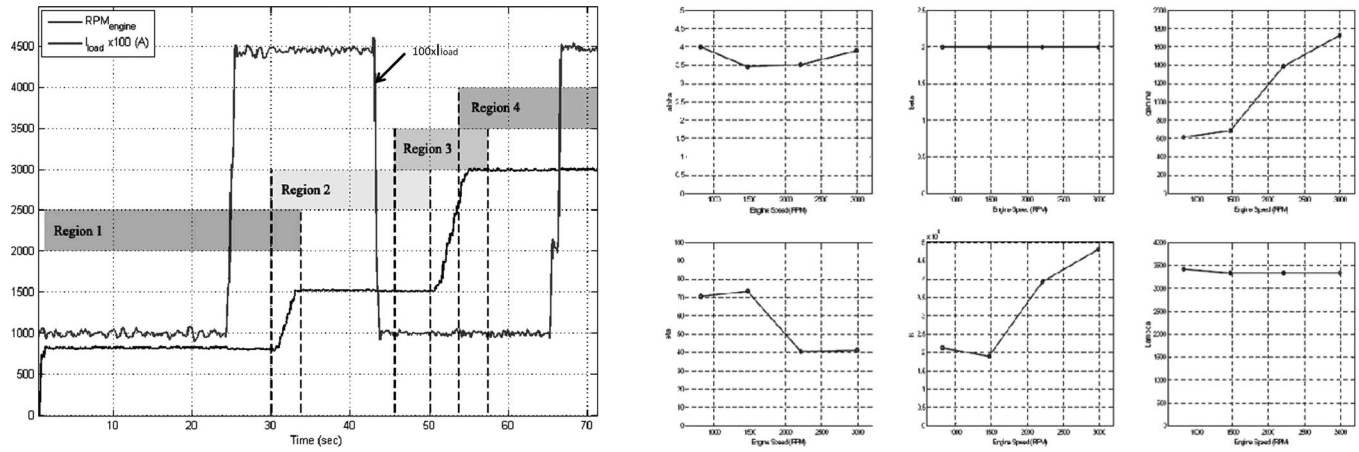

Fig. 9. Automotive EPGS equivalent model identification: (left) Parameters' estimation procedure based on four overlapping regions, (right) Identified parameters for the equivalent alternator model: α, β, η, γ, κ, λ.

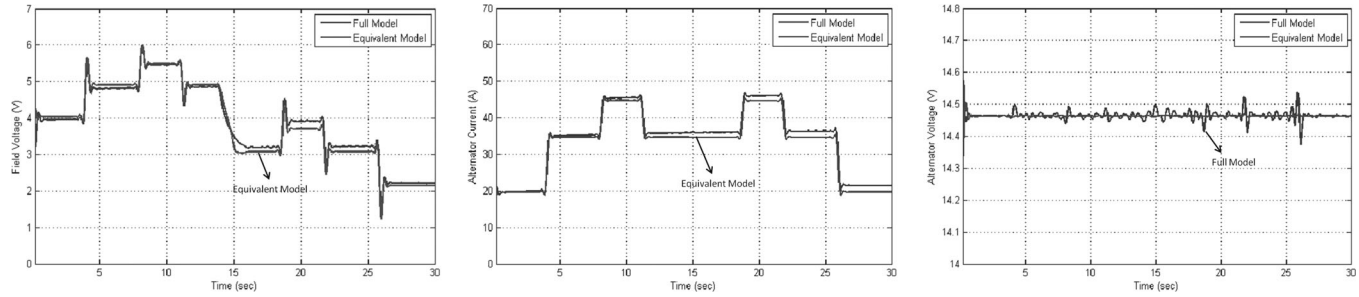

Fig. 10. Automotive EPGS equivalent model validation: (left) field voltage, (middle) alternator current, and (right) alternator voltage.

where $I_{\rm dc}^{\rm nom}$ is the nominal alternator current, chosen as 120 [A], and $V_{\rm ref}^{\rm nom}$ is the nominal reference voltage, chosen as 14.46 [V]. The fault diagnosis process is illustrated in Fig. 12.

Fault diagnosis process is based on the following assumptions: 1) alternator output current $I_{\rm dc}$ is known; 2) the field voltage V_f, regulator output, is known; and 3) alternator output voltage $V_{\rm dc}$ is measured. It is important to notice that the equivalent model is used as an open-loop estimator for the full model without fault. The behavior of the equivalent model is not affected by faults. Under the assumption of a single fault occurrence, fault signature and fault isolation strategy can be described by the fault signatures

$$\text{sig}_{r_1} = \begin{cases} 1, & \text{if std}(r_1) > h_1 \\ 0, & \text{if std}(r_1) < h_1 \end{cases} \tag{22}$$

$$\text{sig}_{r_2} = \begin{cases} 1, & \text{if mean}(r_2) > h_2 \\ 0, & \text{if mean}(r_2) < h_2 \end{cases} \tag{23}$$

$$\text{sig}_{r_3} = \begin{cases} 1, & \text{if mean}(r_3) > h_{3,\rm up} \\ -1, & \text{if mean}(r_3) < h_{3,\rm down} \\ 0, & \text{else} \end{cases} \tag{24}$$

and fault isolation logic are shown in Table II, respectively.

In (22)–(24), std$(\cdot)$ stands for the standard deviation function over a time period, mean$(\cdot)$ stands for the average function over a time period, and in Table II, the sign "x" indicates "don't care." To decrease the false alarm that may be caused by noise or transient change of load current or engine speed, we used window-based averaging for signature calculation. Such averaging reduces effects of noise and model error on detection, and, therefore, reduces probability of a false alarm.

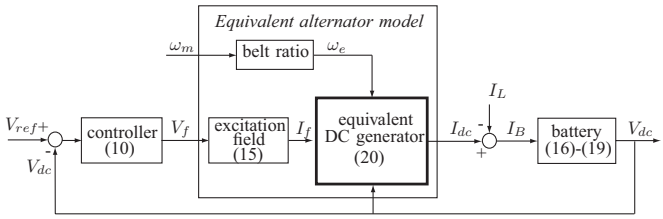

Fig. 11. Need of an equivalent alternator model: Block diagram of the automotive EPGS system with an equivalent alternator model (DC machine in the orange box).

TABLE II
FAULT ISOLATION LOGIC

r_1	r_2	r_3	*Fault Type*
0	1	0/-1	Belt slippage
0	x	1	Voltage regulator (increased V_{ref})
0	0	-1	Voltage regulator (drop V_{ref})
1	x	x	Power Electronics (diode fault)
0	0	0	None

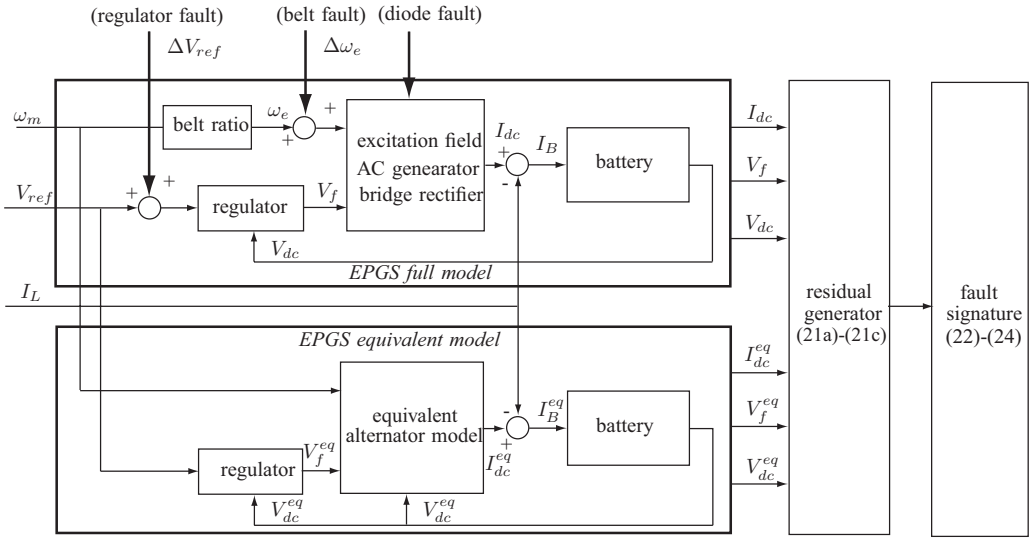

Fig. 12. Model-based fault diagnostic scheme for an automotive alternator.

C. Threshold Selection and Calibration

Residual processing is a very important part of the FDI scheme. In fact, because of model inaccuracy, disturbance, or measurement noise, conditions for perfectly robust residual generation cannot be met in practice. Thus, it is important to be able to systematically design detection thresholds to make decisions from residuals. Optimal threshold selection that is based on statistical hypothesis testing is a commonly used threshold selection method [23].

1) Optimal Threshold Selection Method: The optimal threshold selection method is based on statistical hypothesis testing concepts [24] where residuals are viewed as a sequence of independent random variables. Residuals corresponding to normal operation are assumed to be randomly distributed under the *hypothesis H_0 (no fault)*, while residuals corresponding to a faulty condition are assumed to be randomly distributed under *hypothesis H_1 (faulty)*. Thus, the binary hypothesis test is made.

Let r be the random variable corresponding to a residual. The rule adopted most commonly is that whenever a sample of random variable r is above threshold value, hypothesis H_1 is chosen, whereas H_0 is selected if the sample is below the threshold. If the pdf associated with r under each hypothesis is known, we can compute various probabilities that are relevant in the context of fault diagnosis.

We can define the following.

1) *Probability of detection (P_D):* the probability that we choose hypothesis H_1 when H_1 is indeed the correct hypothesis. It can be defined by

$$P_D = \int_h^\infty p_1(x)dx \tag{25}$$

where h is the selected threshold, and p_1 is the pdf of the random variable r under hypothesis H_1.

2) *Probability of a false alarm (P_F):* the probability that we choose hypothesis H_1 when H_0 is the correct hypothesis. It can be defined by

$$P_F = \int_h^\infty p_0(x)dx \tag{26}$$

where h is the selected threshold, and p_0 is the pdf of the random variable r under hypothesis H_0.

3) *Probability of a misdetection (miss) (P_M):* the probability that we choose hypothesis H_0 when H_1 is the correct hypothesis. It can be defined by

$$P_M = \int_{-\infty}^h p_1(x)dx \tag{27}$$

where h is the selected threshold, and p_1 is the *pdf* of the random variable r under hypothesis H_1.

Optimal threshold selection should result in P_D as high as possible and P_F and P_M as low as possible. However, these objectives are usually conflicting in real applications. Thus, the threshold selection problem is always a tradeoff between miss detection and false alarms. A practical but effective way to obtain the statistical optimal threshold is by minimizing total probability of error $(P_F + P_M)$.

IV. Validation of Diagnosis for the Electric Power Generation and Storage system

In this section, we illustrate the experimental setup that is used for the validation of the EPGS system and its diagnostics algorithms. In addition, experimental results of threshold selection and calibration and diagnostic algorithms are shown and discussed.

A. Experimental Setup and Electric Power Generation and Storage Faults Simulation

The test bench setup provides a reliable validation platform for a real electrical power generation system and allows simulation of component faults and validation of the EPGS model and the EPGS fault diagnosis algorithms. A schematics of an EPGS

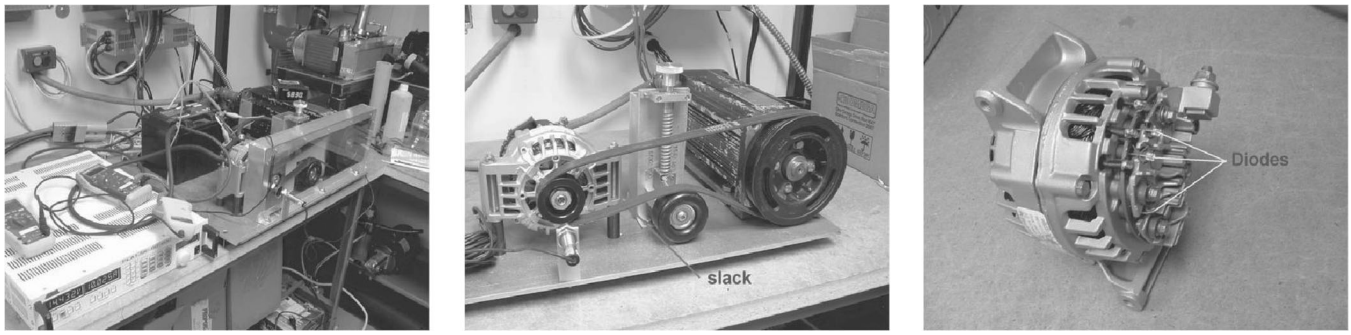

Fig. 13. Experimental setup and EPGS faults simulation by the test bench: (left) Part of the EPGS test bench setup at The Ohio State University Center of Automotive Research, (middle) belt fault, and (right) diode fault.

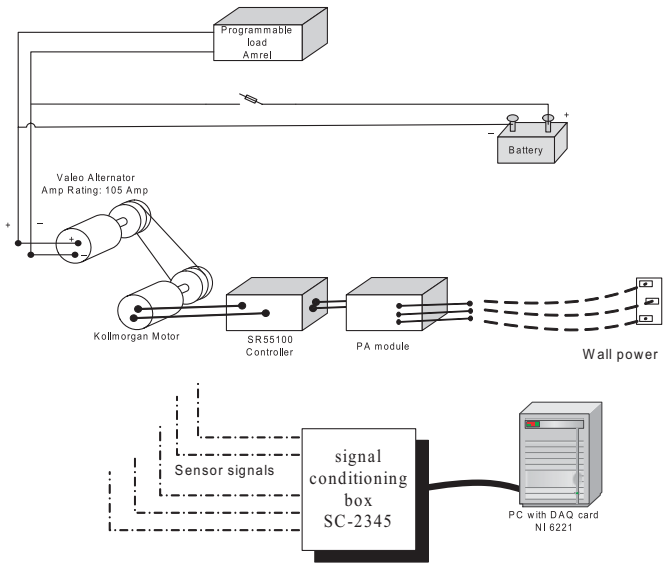

Fig. 14. Schematics of the EPGS test bench, including an electric motor, a vehicle alternator, a programmable power load, and a 12-V lead-acid battery.

test bench is provided in Fig. 14. The automotive EPGS experimental test bench, used in this study, is located at The Ohio State University Center for Automotive Research, as depicted on the left of Fig. 13, and it is mainly composed of an electric motor, a vehicle alternator, a programmable power load, and a 12-V lead-acid battery. In the test bench used in this study, electric motor speed can be controlled by serial communication; therefore, it is used to simulate engine rotation performance. Programmable electric load is used to simulate vehicle load demands by running a predefined load current profile. The electric load can also be remotely controlled by serial communication. The battery and alternator work together to provide current demanded by the load. The test bench data acquisition (DAQ) system was developed on MATLAB DAQ toolbox; it provides a seamless linkage between DAQ and data analysis in the MATLAB environment. The developed DAQ system collects all selected signals: alternator voltage, alternator current, battery voltage, battery current, load current, motor RPM, alternator RPM, and alternator field voltage. The DAQ system is also used to control motor speed and electric load current level as programmed. An important function of the test bench is to simulate EPGS faults encountered in real vehicles in order to validate designed diagnostic algorithms. The belt fault, rectifier diode open fault, and voltage regulator fault are considered as EPGS system faults in this study. The simulation of two kinds of EPGS faults has been made possible on the test bench: belt slip fault and diode fault, as shown in the middle and right of Fig. 13. For alternator belt slip fault simulation, a manually tunable idler is used between the alternator and motor pulley. By adjusting the position of the idler, the tightness of the belt can be controlled precisely. A common fault with the alternator rectifier is a diode fault. The diode may be damaged by high voltage or other causes. With the test bench, this kind of fault can be realized by cutting off the connection wire of one diode. For convenience of operation, a manual switch can be added to the diode connection wire. Therefore, by turning the switch ON or OFF, we can alternate easily between no fault and diode fault condition.

B. Threshold Selection Experimental Results

Threshold selection is crucial to the accuracy and robustness of any diagnostic system. For this reason, we developed a reliable and accurate model of the EPGS, and then we spent time quantifying uncertainty in the model. There was clear separation between residual distribution under normal conditions and under faulty ones. In the experimental validation, many tests using design of experiment (DOE) methodology were conducted. However, because of article size limitation, only one example of these tests is shown and discussed.

From the signature equations (22)–(24), four thresholds needed to be calibrated: h_1, which is related to the belt slip fault, h_2, which is related to rectifier diode fault, and $h_{3,\mathrm{up}}$ and $h_{3,\mathrm{down}}$, which are related to regulator fault. With the EPGS test bench, we are able to simulate the fault in the belt and in the rectifier. In this paper, we only calibrate thresholds h_1 and h_2, while assuming for residual thresholds $h_{3,\mathrm{up}}$ and $h_{3,\mathrm{down}}$ values of (0.04) and (-0.04), respectively.

To apply the threshold selection methods introduced previously, an extensive number of experimental tests were conducted to generate the estimation of a residual pdf. Thresholds h_1 and h_2 are selected by the statistical optimal threshold method, and their final values are 0.053 and 0.13, respectively (see Fig. 15).

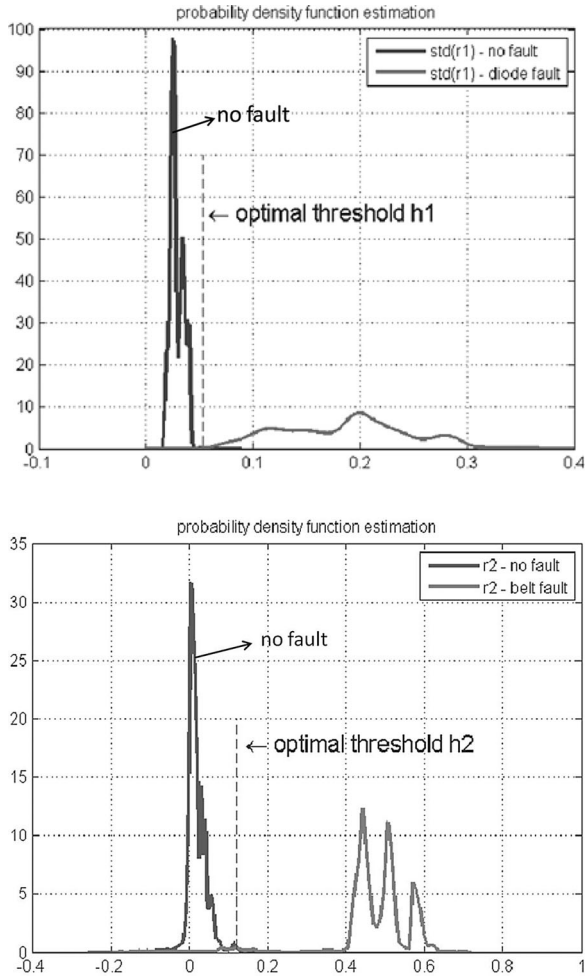

Fig. 15. Statistical optimal thresholds: h_1 (top) and h_2 (bottom).

C. Electric Power Generation and Storage Diagnostics Experimental Results

In this section, we present experimental results of the diagnosis of two components of the alternator (belt slip and diode bridge rectifier). Experimental evaluation results were obtained for diagnosis of the three faults. However, because of article size limitation, only diode and belt faults have been discussed. Regulator fault and corresponding threshold calibration are more straightforward than the other two faults.

After threshold calibration is performed, effectiveness of the EPGS diagnosis strategy and the selected threshold needs to be experimentally validated. The experimental validation of the fault diagnosis algorithm is carried out offline and following the scheme in Fig. 16.

In the validation phase, it is important to check diagnostic system performance under all possible operating conditions both normal and faulty. A DOE methodology is adopted to validate performance of the system and selected threshold values. In this paper, because of size limitation, only one example of validation was shown and discussed. In particular, a combined 180 s experimental data are used as a diagnosis validation example. Input profiles, which are shown in Fig. 17, are composed of three identical sections.

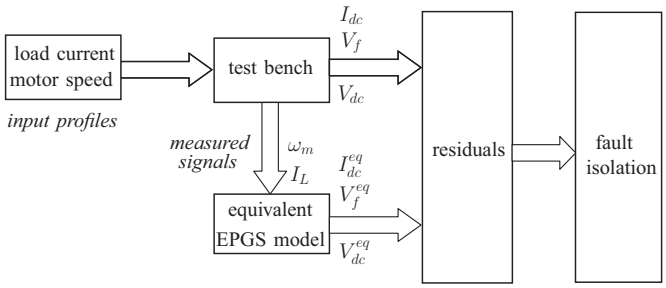

Fig. 16. Experimental validation: Block diagram of the EPGS diagnostics validation process.

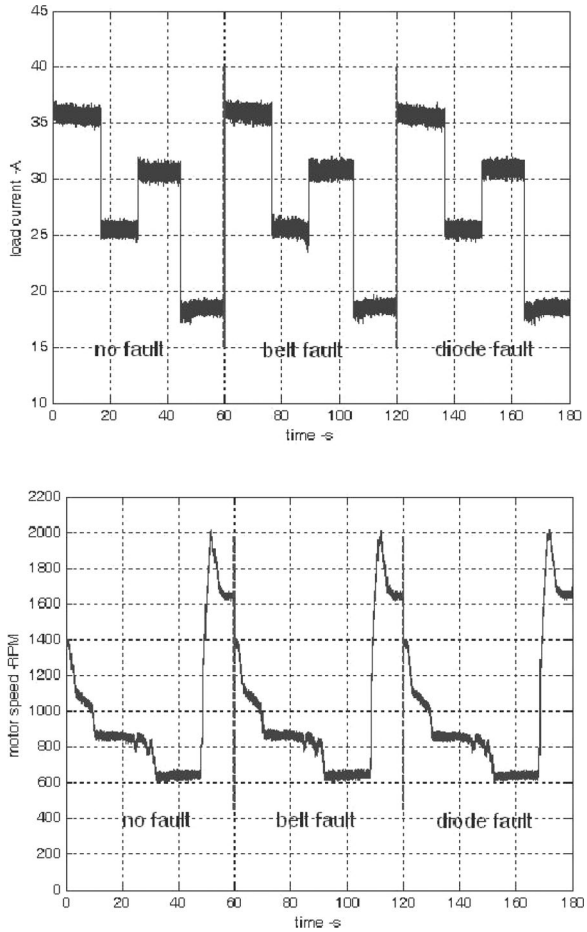

Fig. 17. Experimental validation of the EPGS diagnosis: Load current input profile (top) and motor speed input profile (bottom).

For the first 60 s, no fault happens; during 60–120 s, a short belt slip fault is introduced from 80 to 88 s; from 120 to 180 s, the diode fault is injected on the whole period. The generated fault residual and corresponding fault signature are shown in Fig. 18. Checking with fault isolation logic given in Table II, we can conclude that for the first 60 s, no fault is detected; from 80 to 90 s, a belt slip fault is detected; and from 120 to 180 s, a diode fault is detected. The conclusions match exactly with the experimental setup. Correct FDI of this validation shows effectiveness of the fault diagnosis algorithm and threshold selection methods.

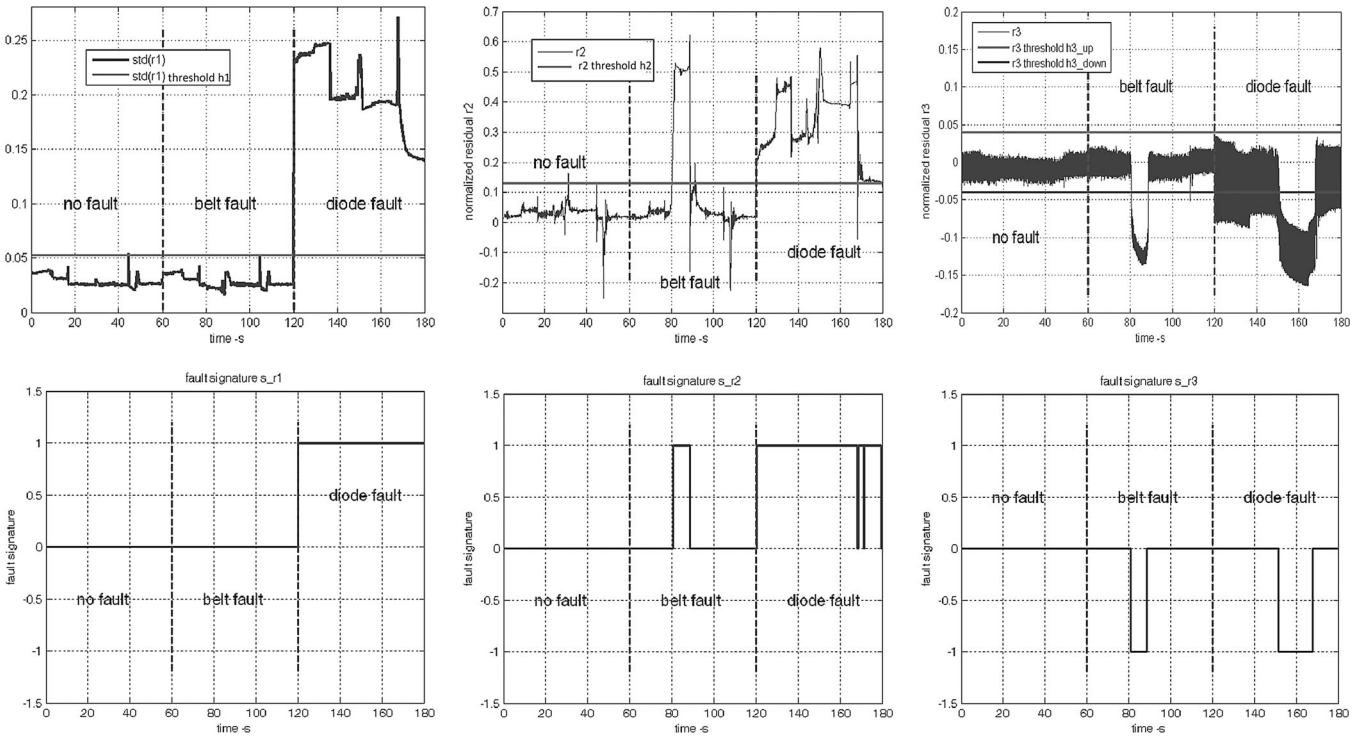

Fig. 18. Experimental validation of the EPGS diagnosis: residuals (top) and fault signatures (bottom).

V. Conclusion and Future Work

This conclusive section presents a summary of the main accomplishments presented in this paper, and a description of further investigations of this research. Main contributions of this paper are as follows:

1) development and experimental validation of an accurate EPGS system model;
2) development and experimental validation of an equivalent simplified model of the alternator and, then, of the EPGS system;
3) design, implementation, and experimental validation of a robust diagnostics for belt and diode faults;
4) application of an optimal threshold selection and calibration method based on statistical analysis of experimental tests.

Experimental results showed that the diagnosis strategy is effective in detecting and isolating the belt slipping fault and the diode bridge rectifier fault.

Main future work that should be conducted in this research includes the following:

1) expansion of the diagnostic system to include other alternator faults, such as winding and bearing faults;
2) design a hierarchical diagnosis algorithm that takes into account sensor and battery faults;
3) integration of alternator diagnosis with other diagnostics, including battery and sensors;
4) development of a supervisory diagnostics system for the vehicle power system;
5) validation of the diagnostics algorithm onboard in a real vehicle environment.

Acknowledgment

The authors would like to thank General Motors for the financial and technical support and the people of the laboratory and facilities at the Center for Automotive Research, The Ohio State University, Columbus, for their assistance with the experiments. In particular, they thank C. Suozzo. They would also like to thank Prof. P. Pisu of Clemson University, Clemson, SC, for his valuable discussions and support during the first phase of this study, and Prof. D. J. Perreult of the Massachusetts Institute of Technology, Cambridge, for his kind help during bibliographic review.

References

[1] V. Caliskan, "Modeling and simulation of a claw-pole alternator: Detailed and average models," Laboratory for Electromagnetic and Electronic Systems, Massachusetts Institute of Technology, Cambridge, Tech. Rep. 00-009, Oct. 12, 2000.

[2] H. Bai, S. Pekarek, J. Tichenor, W. Eversman, D. Buening, G. Holbrook, M. Hull, R. Krefta, and S. Shields, "Analytical derivation of a coupled-circuit model of a claw-pole alternator with concentrated stator windings," *IEEE Trans. Energ. Convers.*, vol. 17, no. 1, pp. 32–38, Mar. 2002.

[3] V. Caliskan, D. J. Perreault, T. M. Jahns, and J. G. Kassakian, "Analysis of three-phase rectifiers with constant-voltage loads," *IEEE Trans. Circuits Syst. I, Fundam. Theory Appl.*, vol. 50, no. 9, pp. 1220–1227, Sep. 2003.

[4] G. D. Marques, "A simple and accurate system simulation of three-phase diode rectifiers," in *Proc. 24th Annu. Conf. IEEE Ind. Electron. Soc.*, Aug. 31–Sep. 4, 1998, pp. 416–421.

[5] G. Henneberger and S. Kuppers, "Field calculation and dynamic simulation of a claw-pole alternator," in *Proc. 7th Int. Conf. Electr. Mach. Drives*, Durham, U.K., Sep. 11–13, 1995, pp. 286–290.

[6] S. C. Tang, T. A. Keim, and D. J. Perreault, "A thermal modeling of Lundell alternators," *IEEE Trans. Energ. Convers.*, vol. 20, no. 1, pp. 25–36, Mar. 2005.

[7] Z. M. Salameh, M. A. Casacca, and W. A. Lynch, "A mathematical model for lead-acid batteries," *IEEE Trans. Energ. Convers.*, vol. 7, no. 1, pp. 93–98, Mar. 1992.

[8] A. Ferreira, J. Pomilio, G. Spiazzi, and L. de Araujo Silva, "Energy management fuzzy logic supervisory for electric vehicle power supplies

system," *IEEE Trans. Power Electron.*, vol. 23, no. 1, pp. 107–115, Jan. 2008.

[9] H. Blanke, O. Bohlen, S. Buller, R. W. De Doncker, B. Fricke, A. Hammouche, D. Linzen, M. Thele, and D. U. Sauer, "Impedance measurements on lead-acid batteries for state-of-charge, state-of-health and cranking capability prognosis in electric and hybrid electric vehicles," *J. Power Sources*, vol. 144, no. 2, pp. 418–425, 2005.

[10] F. Huet, "A review of impedance measurements for determination of the state-of-charge or state-of-health of secondary batteries," *J. Power Sources*, vol. 70, no. 1, pp. 59–69, 1998.

[11] M. Urquidi-Macdonald and N. A. Bomberger, "Predicting failure of secondary batteries," *J. Power Sources*, vol. 74, no. 1, pp. 87–98, 1998.

[12] J. Yan, W. Li, and Q. Zhan, "Failure mechanism of valve-regulated lead-acid batteries under high-power cycling," *J. Power Sources*, vol. 133, no. 1, pp. 135–140, 2004.

[13] E. Meissner and G. Richter, "Battery monitoring and electrical energy management: Precondition for future vehicle electric power systems," *J. Power Sources*, vol. 116, no. 1–2, pp. 79–98, 2003.

[14] X. Zhang, H. Uliyar, L. Farfan-Ramos, Y. Zhang, and M. Salman, "Fault diagnosis of automotive electric power generation and storage systems," in *Proc. Int. Conf. Control Appl.*, Yokohama, Japan, Sep. 8–10, 2010, pp. 719–724.

[15] Y. Zhang, S. Rajagopalan, and M. Salman, "A practical approach for belt slip detection in automotive electric power generation and storage system," presented at the Aerosp. Conf., Big Sky, MT, Mar. 6–13, 2010.

[16] M. M. Hamdan, G. Holler, K. A. Grolle, J. M. Macnamara, and K. A. Thakkar, "System and method for detecting alternator condition," U.S. Patent 6 862 504, 2005.

[17] A. Moyes, G. M. Burt, J. McDonald, J. R. Capener, J. Dray, and R. Goodfellow, "The application of expert systems to fault diagnosis in alternators," in *Proc. 7th Int. Conf. Electr. Mach. Drives*, 1995, pp. 171–175.

[18] A. Scacchioli, G. Rizzoni, and P. Pisu, "Model-based fault diagnosis design for an electrical automotive system," in *Proc. Int. Mech. Eng. Congr. Expo. ASME Dynam. Syst. Control Div.*, Chicago, IL, Nov. 5–10, 2006, pp. 315–324.

[19] A. Scacchioli, G. Rizzoni, and P. Pisu, "Hierarchical model based fault diagnosis for an electrical power generation storage automotive system," in *Proc. 26th IEEE Amer. Control Conf.*, New York City, NY, Jul. 11–13, 2007, pp. 2991–2996.

[20] W. Li, C. Suozzo, S. Onori, G. Rizzoni, M. A. Salman, and F. Zhang, "Experimental calibration and validation of fault diagnosis of automotive electric power generation system," in *Proc. ASME Dynam. Syst. Control Conf.*, Ann Arbor, MI, Oct. 20–22, 2008, pp. 1317–1324.

[21] K. B. S. HanSung, "Dynamic battery modeling in hybrid electric vehicles," M.S. Thesis, Dept. Mech. Eng., The Ohio State University, Columbus, 2002.

[22] C. De-Shiou, "Sliding mode observers for automotive alternators," Ph.D. dissertation, Dept. Electr. Eng., The Ohio State University, Columbus, 1998.

[23] J. Chen and R. J. Patton, *Robust Model-Based Fault Diagnosis for Dynamic Systems*. Boston, MA: Kluwer, 1999.

[24] H. L. Van Trees, *Detection, Estimation, and Modulation Theory*. New York: Wiley, 1958.

Annalisa Scacchioli (M'04) received the *Laurea* degree in electrical engineering and the Ph.D. degree in electrical engineering and computer sciences from the University of L'Aquila, L'Aquila, Italy, in 2000 and 2005, respectively.

She is a Visiting Assistant Professor of mechanical engineering with New York University (NYU) School of Engineering. Before joining NYU, she was a Postdoctoral Researcher with the Center for Automotive Research, The Ohio State University, from 2005 to 2006, with the Department of Civil and Environmental Engineering, University of California at Berkeley, from 2007 to 2008, and with the *Daniel Guggenheim* School of Aerospace Engineering, Georgia Institute of Technology, from 2008 to 2010, and a Visiting Researcher with Ford Motor Company's Research and Advanced Engineering, Dearborn, MI, from 2008 to 2010. Her research interests include the broad and interdiscliplinary area of modeling, identification, feedback, control, and diagnosis applied to complex-engineered systems, with focus on automotive, civil-structural, and air-transportation systems.

She is a member of the International Federation of Automatic Control and the American Society of Mechanical Engineers.

Giorgio Rizzoni (F'04) received the B.S., M.S., and Ph.D. degrees from the University of Michigan, Ann Arbor, in 1980, 1982 and 1986, respectively, all in electrical and computer engineering.

He is the Ford Motor Company Chair in electromechanical systems, and a Professor with the Departments of Mechanical and Aerospace and Electrical and Computer Engineering, The Ohio State University, Columbus, where since 1999, he has been the Director of the Center for Automotive Research, an interdisciplinary university research center with the Ohio State University College of Engineering. His research interests include future ground vehicle propulsion systems, including advanced engines, electric and hybrid-electric drivetrains, advanced batteries, and fuel cell systems.

Dr. Rizzoni became a Fellow of the Society of Automotive Engineers in 2005. He is the recipient of the 1991 National Science Foundation Presidential Young Investigator Award, and of several other technical and teaching awards.

Mutasim A. Salman (SM'08) received the Bachelor's degree in electrical engineering from the University of Texas at Austin, Austin, and the M.S. and Ph.D. degrees in electrical engineering with specialization in systems and control from the University of Illinois at Urbana-Champaign, Urbana-Champaign. He also received the executive M.B.A. degree from Michigan State University.

In 1984, he joined the GM R&D staff, Warren, MI, where he is currently a Laboratory Group Manager and a Technical Fellow with the Electrical and Controls Integration Laboratory, General Motors (GM) Research and Development Center. He is responsible for the development and validation of algorithms for state of health monitoring, diagnosis, prognosis, and fault tolerant control of vehicle critical systems. He has pioneered the work on integrated chassis control in the late 1980s that led to the production of GM "Industry First" Stabilitrak1 and then to Stabilitrak3. He has extensive experience in hybrid vehicle, modeling, control, and energy management strategies. He holds 36 patents of which seven of them have already been used in products. He has coauthored more than 56 refereed technical publications and a book.

Dr. Salman has several GM awards that include four GM prestigious Boss Kettering, three McCuen, and two President and Chairman awards.

Weiwu Li received the B.S. degree in mechanical engineering from Jilin University, Changchun, China, in 1997, the M.S. degree in mechanical engineering and the Ph.D. degree in control engineering from Zhejiang University, Hangzhou, China, in 2000 and 2004, respectively, and the M.S. degree in mechanical engineering from The Ohio State University, Columbus, in 2008.

He is currently a Research Engineer with Cummins, Columbus, IN, working on alternative fuel engines.

Simona Onori (M'11) received the *Laurea* degree (*summa cum laude*) from the Department of Electrical and Computer Engineering, University of Rome "Tor Vergata," Rome, Italy, the M.S. degree in electrical engineering from the University of New Mexico, Albuquerque, and the Ph.D. degree in control engineering from the University of Rome "Tor Vergata," in 2003, 2004, and 2007, respectively.

She is a Research Scientist with the Center for Automotive Research, The Ohio State University (OSU), where she is also a Lecturer with the Department of Mechanical and Aerospace Engineering. Her research interests include control system theory and applications. Her research is focused on model-based control design for advanced propulsion systems, energy management control, and optimization in hybrid electric vehicles (HEVs) and plug-in HEVs, fault diagnosis, and prognosis for automotive system applications, aging, characterization, modeling, and identification of advanced batteries.

Dr. Onori serves as an Associate Editor for the American Society of Mechanical Engineers' Dynamic Systems and Control Conference and American Control Conference, the Guest Editor for the *International Journal of Powertrain*, and an Associate Editor for the *Society of Automotive Engineer's Journal of HEVs*. She is the recipient of the 2012 Lumley Interdisciplinary Research Award by the OSU College of Engineering and TechColumbus 2011 Outstanding Technology Team Award.

Xiaodong Zhang (M'02) received the B.S. degree from the Huazhong University of Science and Technology, Wuhan, China, in 1994, the M.S. degree from Shanghai Jiao Tong University, Shanghai, China, in 1997, and the Ph.D. degree from the University of Cincinnati, Cincinnati, OH, in 2001, all in electrical engineering.

He is currently an Associate Professor with the Department of Electrical Engineering, Wright State University, Dayton, OH. Before joining Wright State University, he had more than five years of industrial experience. He was a Senior Researcher with General Motor's Research and Development Center, Warren, MI, and a Program Manager for control and diagnostics with Intelligent Automation Inc., Rockville, MD. His research interests include intelligent control systems, fault diagnosis and prognosis, fault-tolerant control, and cooperative and distributed control.

Dr. Zhang is an Associate Editor of the IEEE TRANSACTIONS ON CONTROL SYSTEMS TECHNOLOGY and a member of the International Federation of Automatic Control SAFEPROCESS Technical Committee.